Pertanika J. Sci. & Technol. 28 (4): 1487 - 1515 (2020)

PERTANIKA JOURNALS

SCIENCE & TECHNOLOGY

Journal homepage: http://www.pertanika.upm.edu.my/

Seasonal Upwelling in the Northern Arafura Sea from Multi-datasets in 2017

Agus Saleh Atmadipoera[1]*, Agits Agnia Almatin[1], Rina Zuraida[2] and Yani Permanawati[3]

[1]Department of Marine Science and Technology, Faculty of Fisheries and Marine Sciences, IPB University, 16680 Bogor, West Java, Indonesia
[2]Center for Geological Survey, Geological Agency, 40122 Bandung, Indonesia
[3]Marine Geological Institute, Balitbang ESDM, 40174 Bandung, Indonesia

ABSTRACT

Seasonal upwelling phenomenon in the Arafura Sea plays an important role on supplying upwelled nutrient-rich water to sustain biogeochemistry processes and thus contributes to high marine primary productivity and fisheries resources in this region. The objective of this research was to investigate physical process and dynamics of upwelling by analyzing stratification of seawater properties, evolution of surface ocean-atmosphere parameters, and current structure and transport volume in the northern Arafura Sea. The multi-datasets in 2017 were used in this study, acquired from field CTD measurement, satellite-derived sea surface parameters, and the ocean general circulation model outputs, which were processed and analyzed using the available standard procedure. It was found that upwelling event was associated with a sharp subsurface thin layer that upsloping isotherms (23.5 - 25.5 °C), isohalines (33.50 - 34.25 psu), and isopycnals (21.8 - 23.2 kg/m^3) from the shelf-break region to the inner shelf region at a distance of approximately 167 km. This barrier layer separated the first surface mixed layer from the second mixed layer beneath the subsurface layer. The model suggests that the current in these two layers is in the opposite direction, to the west in the first layer as a response to the Ekman drift and to the

ARTICLE INFO

Article history:
Received: 5 April 2020
Accepted: 27 July 2020
Published: 21 October 2020

DOI: https://doi.org/10.47836/pjst.28.4.19

E-mail addresses:
atmadipoera_itk@apps.ipb.ac.id (Agus Saleh Atmadipoera)
agits.agnia@gmail.com (Agits Agnia Almatin)
rina.zuraida@grdc.esdm.go.id (Rina Zuraida)
yani.permanawati@esdm.go.id (Yani Permanawati)
*Corresponding author

ISSN: 0128-7680
e-ISSN: 2231-8526

east in the second layer as a current extension from deep Aru basin. Therefore, upwelling dynamics here is not only generated by the southeasterly monsoon winds from May (onset) to November (termination) that transport warm and fresh surface water away from the shelf, but also modulated by the presence of strong inflow currents beneath subsurface that supply colder saltier nutrient-rich water into the shelf. During the upwelling period, mean transport volume in the upper 25 m depth between Aru and Papua at 134.25°E was -0.28 (±0.34) Sv (westward), but the transport volume between 25m and 110m depth was +1.06 (±0.29) Sv (eastward), suggesting this inflow may regulate the upwelling and supply Arafura shelf water.

Keywords: Arafura sea, chlorophyll-a, ocean current, salinity, temperature, upwelling

INTRODUCTION

The shallow Arafura shelf sea is located in the eastern Indonesian Archipelago and northern Australia waters, and is a semi-enclosed sea with complex bathymetry ranging from 30 to 90 m depth. The northern part of Arafura Sea faces on eastern deep Banda Sea and Aru basin with high pelagic and demersal fisheries productivity. Arafura and eastern Timor Seas show a seasonal high marine productivity and abundance of marine living resources with primary productivity greater than 300 gC/cm2/year (Alongi et al., 2011). This high marine productivity is associated significantly with upwelling phenomenon (Alongi et al., 2011). Hence, Arafura Sea is one of important fishing grounds in Indonesia, contributing 21% of marine fisheries at about 2.64 million ton/year (Sari et al., 2018).

Upwelling is defined simply as a physical oceanographic process in which displaced surface warmer waters are replaced by colder and nutrients-rich water that wells up from deeper layer, and its major driving factor is surface wind fields (Sarhan et al., 2000). According to Wyrtki (1961) upwelling event in Arafura Sea is categorized as a seasonal coastal upwelling, which is driven by the southeasterly monsoon winds (Figure 1). Modeling study of Kämpf (2015) assumed that upwelling in Arafura Sea was forced by eastward flow of under-currents derived from eastern Banda slope and westward flow in the surface layer. A schematic surface circulation during the southeast monsoon (SEM) period from May to September (Figure 1) is indicated by westward and southwestward flows as a response to the southeasterly monsoon winds (Wyrtki, 1961; Condie, 2011; Kämpf, 2015).

In some interior Indonesian seas such as Banda Sea, southern Makassar Strait, and Banggai Maluku Sea, the major forcing of coastal upwelling is generated by the persistent southeasterly monsoonal winds which is fully developed during the SEM period, and peak of upwelling period usually appears between August and September. Gordon and Susanto (2001) reported that Banda upwelling was caused by a surface layer divergence in eastern

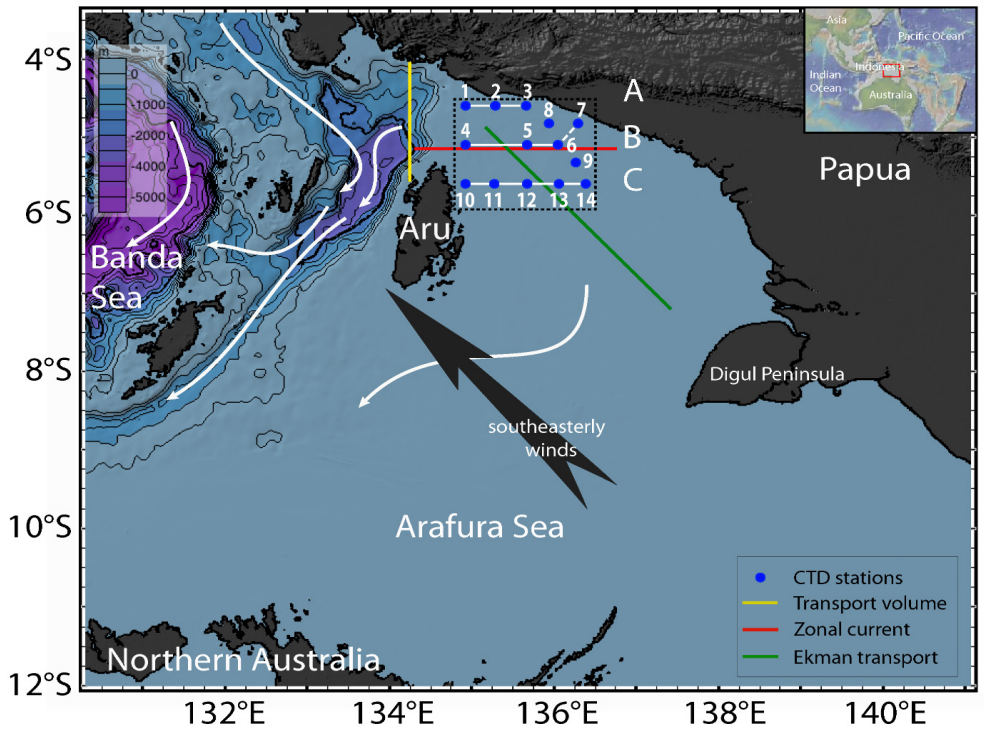

Figure 1. A schematic surface current circulation (white arrows) and southeasterly monsoonal winds (black large arrow) during the Southeast Monsoon (SEM) period over the study area. Bathymetric contours in the Arafura and Banda Sea are drawn for every 500 m. Yellow, red, and green section lines denote for upper 25 m transport volume in east-west direction, depth-distance zonal current section, and Ekman transport calculation, respectively. CTD station measurement is blue dots. Bathymetry map is made with GeoMapApp (www.geomapapp.org).

part of Banda during the SEM period. In southern tips of Makassar Strait, modelling study showed that southeasterly wind-driven upwelling was modulated by southward surface Indonesian Throughflow from and its intensity is also reduced by leakage of inflow from Selayar Strait (Atmadipoera & Widyastuti, 2015). In western Maluku Sea near Banggai waters close to equatorial region, coastal upwelling is forced by fully developed southerly monsoon winds that blow over small islands of Taliabu and Banggai islands creating upwelled water near coastal waters and flowing northward (Atmadipoera et al., 2018).

Coastal upwelling brings colder, higher saline, and nutrients-rich from deeper layer to sea surface. Surfacing of relatively colder water with isotherms of 24.5°C and 26°C from about 60 m depth to the sea surface have been found during peak of upwelling period in southern Makassar Strait and in Banggai waters in Maluku Sea (Utama et al., 2017; Atmadipoera et al., 2018). Regeneration of the upwelled nutrients-rich water are then

utilized by phytoplankton in the photosynthetic processes with chlorophyll-a pigment receives light energy to be chemical energy. Rosdiana et al. (2017) found that at the center area of upwelling in southern Makassar Strait nutrients tended to be low but the chlorophyll-a was high, suggesting that regeneration of nutrients from deeper layer had been used for photosynthesis processes.

Previous studies on upwelling dynamics from satellite data and ocean model in Arafura Sea and its adjacent waters had been done by Condie (2011), Schiller (2011), Kida and Wijffels (2012) and Kämpf (2015). They showed model seasonal circulation driven by the monsoonal winds and barotropic tides around northern coastal of Australia and part of southern Arafura Sea (Condie, 2011). Model circulation in northern Australian Shelf, including Arafura Sea was also done by Schiller (2011), where his main focus was in Australian Shelf and did not discuss Arafura upwelling. Kida and Wijffels (2012) found negative anomaly of sea surface temperature in northern Arafura Sea during the SEM monsoon, associated with seasonal upwelling event. Using 3-dimension hydrodynamics model Kämpf (2015) suggested classical lee effect that created undercurrent which drove nutrients-rich deep water from eastern Banda Sea slope to northern Arafura Sea by about 300 km, and then this deep nutrients-rich water was lifted up to surface layer, as upwelling process. These modeling studies have revealed a better general understanding on upwelling dynamics and circulation in Arafura Sea and its adjacent waters. However, evolution of surface ocean-atmosphere from the onset to the termination of upwelling, observed stratification of seawater properties, and upper-layer transport volume estimate have still less been well understood.

Here, a field hydrological measurement has been carried out onboard research vessel Geomarin III of Marine Geological Institute Bandung Indonesia during the peak on upwelling period, from 2 to 12 September 2017. The objective of present study was to investigate physical processes and dynamics of upwelling in northern Arafura Sea by analyzing stratification of seawater properties, evolution of upwelling, current structure and transport volume estimates from multi-datasets (field observation, satellite-derived parameters, and general ocean circulation model outputs).

MATERIALS AND METHODS

Study Area

The study area was located in the northern Arafura Sea with geographical boundary between longitude of 130°E–141°E and latitude of 4°S–12°S. Figure 1 shows the location of the 12 CTD casts, the dashed black rectangle box and three cross-sections applied in this study, namely section A, B, and C. Black dashed rectangle is a sampling box for data and model validation and extraction of time-series analysis of sea surface temperature (SST), sea surface height anomaly (SSHA), air temperature, and surface chlorophyll-a (chl-a). Red-

line is a cross-section for analysis of depth-longitude zonal current component; yellow-line is for calculation of transport volume in the upper 25 m depth, 25-55 m depth, 55-110 m depth; and northwest-southeast transect (green-line) is for calculating Ekman transport derived from the wind fields datasets (Figure 1).

Data

Field measurement of CTD data casts from sea surface down to near seabed that vary between 43 m and 80 m depth, had been carried out at 12 stations (Table 1). The Sea-Bird Electronics SBE-CTD 19plus with 4 Hz sampling rate (Sea-Bird Scientific, 2017) had been used during the field measurement. The profiling of conductivity-temperature-depth with SBE-CTD can be done when the CTD sensors are lowered (downcast) and lifted up (upcast). However, in this study, only downcast CTD profiling data were used for analysis, since the profiling was not interrupted by bottle rosette stops.

The daily averaged model output datasets (3-dimension zonal and meridional current components, seawater temperature, and salinity) were obtained from simulation results of 1/12° ocean general circulation model of INDESO configuration, performed by CLS

Table 1

Hydrographic CTD measurement during the cruise in the northern Arafura Sea onboard the R.V. Geomarine 3 of Marine Geological Institute Bandung

Station	Geographical coordinate		Date	Local Time (UTC+9)	Bottom depth (m)	CTD depth (m)
	longitude (°E)	latitude (°S)				
1	135.098	4.6123	02/Sep/2017	23.42	80	72
2	135.466	4.61884	03/Sep/2017	03.19	63	57
3	135.816	4.61371	03/Sep/2017	05.25	43	30
4	135.096	5.06561	10/Sep/2017	15.05	75	74
5	135.82	5.0681	03/Sep/2017	15.48	69	65
6	136.132	5.06545	03/Sep/2017	13.59	56	48
7	136.432	4.82533	03/Sep/2017	10.59	43	40
8	136.129	4.8149	03/Sep/2017	08.41	54	53
9	136.37	5.27615	12/Sep/2017	03.54	44	38
10	135.101	5.57434	11/Sep/2017	11.40	60	55
11	135.47	5.58089	11/Sep/2017	22.08	45	42
12	135.819	5.57964	11/Sep/2017	20.10	45	42
13	136.133	5.5745	12/Sep/2017	05.10	52	49

France. Model configuration and validation has been described in detail in Tranchant et al. (2015). INDESO is a program of developing and utilizing oceanographic data for Indonesian fisheries and marine needs, which was developed by the Ministry of Maritime Affairs and Fisheries of the Republic of Indonesia through the Agency of Marine Fisheries Research and Development.

In brief, the configuration of the INDESO model can be described as follows, horizontal resolution of 1/12° or approximately 9.25 km and vertical resolution consisting of 50 depth levels, where at the depth of the first 10 meters, the thickness of the layer is less than 2 meters and then increasing by 10 meters at 50 meters depth; bathymetry of this model from ETOPO2 v2 with a 2-minute grid resolution and from GEBCO with a 1-minute grid resolution; atmospheric forcing used data from operational analysis of the European Center for Medium-Range Weather Forecasts (ECMWF); the ocean-atmosphere interaction model uses the "bulk" formula from CORE; tidal forcing has tidal forces geopotential components M2, S2, N2, and K2 (the main component of semidiurnal tides) and components K1, O1, P1, and Q1 (the main components of diurnal tides); and monthly climatology of freshwater runoff is obtained from freshwater runoff data on the coast and 99 major rivers in Indonesia (Tranchant et al., 2015).

The global ocean OSTIA satellite-derived sea surface temperature datasets were obtained from Marine Copernicus (https://resources.marine.copernicus.eu/). The OSTIA global sea surface temperature reprocessed product provides daily gap-free maps of foundation sea surface temperature and ice concentration (referred to as an L4 product) at 0.05° x 0.05° (5.6 km) horizontal grid resolution and daily-mean temporal resolution, using in-situ and satellite data (Worsfold et al., 2020). The daily-mean of SST datasets in the study area (130-141°E; 4-12°S) were used for the upwelling analysis.

Satellite derived surface chlorophyll-a (chl-a) datasets were also obtained from European Centre for Operational Oceanography of Copernicus in Toulouse France. The daily-mean chlorophyll-a and bio-products refer to chlorophyll-a and primary production (PP) are based on a multi sensors/algorithms approach to provide to end-users the best estimate. Two dailies Chlorophyll-a products are distributed: one limited to the daily observations (called L3), and the other based on a space-time interpolation: the "Cloud Free" (called L4). Products of daily surface chl-a datasets are based on the merging of the sensors SeaWiFS, MODIS, MERIS, VIIRS-SNPP&JPSS1, and OLCI-S3A&S3B with the spatial resolution is 4 km (Copernicus Marine Service, 2019; Garnesson et al., 2019).

Wind-stress datasets in 2017 were derived from scatterometer satellite datasets with 25 km spatial and 6-hour temporal resolutions were obtained from Copernicus Marine Service. In addition, surface atmospheric time-series datasets (zonal and meridional wind speed components, and air temperature) with 6-hour temporal and 0.125° spatial resolutions were obtained from ECMWF (https://www.ecmwf.int/en/forecasts/datasets).

Data Analysis and Validation

The general terminology used for winds fields in the north-south orientation of coastline is cross-shore wind component for zonal (u) and along-shore for meridional (v) components (Emery & Thomson, 2004). However, in northern Arafura Sea where coastline of Papua mainland is oriented northwest-southeast, the wind field components need to be rotated (Figure 1). These schematic rotated wind components represented for the peaks of monsoon period (August and February). Angle of rotation (θ) is estimated by about 58° counter-clockwise from the north (0°) and parallel to the mainland coastline. Rotated zonal (u') and meridional (v') wind-stress components can be calculated as described by Emery and Thomson (2004), and Kutsuwada (1998) (Equation 1):

$$u' = u\cos\theta + v\sin\theta;\ \ and\ \ v' = -u\sin\theta + v\cos\theta \qquad [1]$$

According to Pond and Pickard (1983) and Stewart (2006), offshore Ekman upwelling transport caused by southeasterly monsoon winds can be calculated with the following Equation 2,

$$M_xE = \frac{\tau_y}{f} \qquad \text{and} \qquad M_yE = -\frac{\tau_x}{f} \qquad [2]$$

where, MxE and MyE are along-shore and cross-shore Ekman transport components (kg/m s), respectively; τx and τy are cross-shore and along-shore wind stress component (Pa), respectively; f is Coriolis parameter (rad/s), calculated from f = 2 Ω sin θ; Ω is Earth' rotation speed (7.29x10-5 rad/s); θ is geographical latitude (°).

Estimate of transport total in northern Arafura Sea is calculated by using Ekman transport's approach which is integrated along a transect line, as described by Sprintall and Liu (2005) (Equation 3),

$$Q_E = \Delta x \sum_{i=1}^{n} \frac{\tau_y}{\rho_s f} \qquad [3]$$

where, QE is total Ekman transport (m^3/s); Δx is grid length (m); ρs is density of seawater (1024 kg/m3); n is number of grid (55).

Estimate of transport volume. Transport volume is calculated by integrating zonal current component for each grid (uz,y) to transect length (y) and depth (z), following Emery and Thomson (2004) (Equation 4),

$$Q = \int_{z1}^{z0}\int_{y1}^{y2} u_{z,y}\, dy\, dz \qquad [4]$$

where, Q is transport volume in Sv unit (1 Sv = 106 m^3/s); z is depth integration from sub-surface (z1) of 25 m depth to the sea surface (z0); y is length of section from y1 (4 °S) to y2 (5°24' S) or about 156 km; uz,y is zonal current component (m/s) at depth z and cell y.

Model and data comparison. Deviation of model output from the data measurement is estimated from the root mean square error (RMSE) (Wilks, 2006) (Equation 5),

$$RMSE=\sqrt{\frac{1}{N}\sum_{i=1}^{N}(X\,model_{(i)}-X\,data_{(i)})^2} \quad [5]$$

where, Xmodel(i) is variable of model output (i = 1, 2, 3 …, N); Xdata(i) is variable of data (i = 1, 2, 3 …, N); and N is data number.

Seawater temperature is a key parameter for analysis of upwelling event in the study area. Here, model temperature is compared to observed 12 CTD temperature profiles at the same date and geographical coordinates (colocation). The average of RMSE of temperature from 12 CTD profiles was 0.60 (±0.21)°C. An example of comparison of model and CTD profile is shown in Figure 2. Here, both model and CTD temperature was in good agreement with RMSE of 0.22°C (Figure 2). Difference of model temperature and CTD data at 0.5 m depth was about 0.20°C. Below 35 m depth, both model and data temperature were just overlaid.

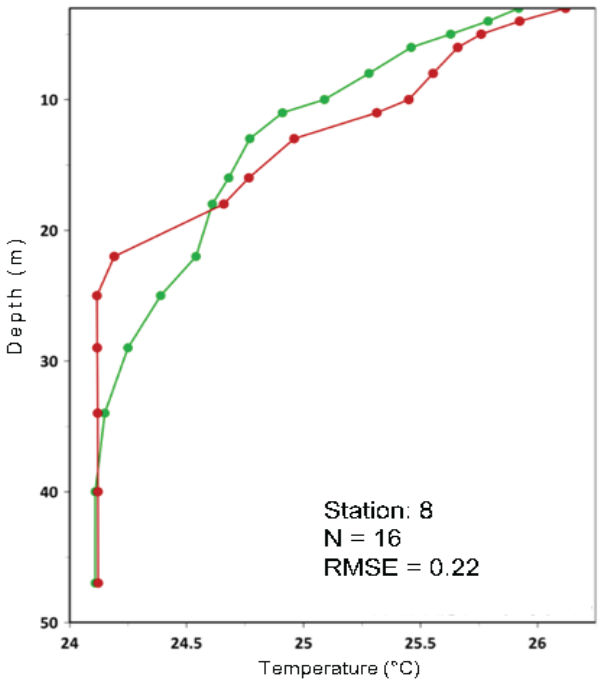

Figure 2. An example for comparison of temperature profiles between model (green) and CTD data (red) at CTD station 8

These small differences may be related to different spatial-temporal resolution between model and CTD data, e.g., model spatial resolution is 9.25 km with daily average, while CTD data is at one-point measurement and very short time snapshot. Since CTD data was only a snapshot field measurement between 2 and 12 September 2017, model temperature datasets were used to evaluate evolution of temperature prior to – during – and after the upwelling event in year 2017.

RESULTS AND DISCUSSION

Evolution of Surface Ocean Parameters: Onset and Termination of Upwelling

Onset and termination of upwelling in Arafura Sea were analyzed from several key ocean-atmosphere parameters, such as surface wind field, SSH, SST, air temperature (Ta), and surface chl-a (Figure 3). The southeasterly monsoon winds predominate from May to October (the SEM period), which are much stronger and much persistent compared to that during the northwesterly monsoon winds – the NWM period (November-April) (Figure 3a). Here, if we apply the Ekman upwelling theory, the southeast monsoon period from May to October is proposed as the onset and termination of upwelling event (in 2017). This is also consistent with other key parameters that fluctuate consistently with the winds data.

Negative anomaly of SSH commenced in May and its minimum was found by about -0.18 cm in August/September, then recovered to positive anomaly of SSH from October to April as under the period of the NMW. Gordon and Susanto (2001) found minimum of anomaly of SSH of about 20 cm (Figure 3b). This minimum of negative SSH anomaly is caused by upwelling process (Kämpf, 2016). The SEM period is also indicated by negative anomaly of SST from June to October with its minimum of -3.0°C in August/September (Figure 3c). Positive anomaly of SST is found during the rest of months (the NWM period). Fluctuation of negative air temperature anomaly (Ta) is similar with anomaly of SST (Figure 3d). However, during the NWM period fluctuation of Ta anomaly is completely different to SST anomaly (Figure 3d). Cooling air temperature may be caused by change of air-sea heat flux over the upwelling area (Sproson & Sahlée, 2014). Fluctuation of chl-a anomaly is out-of-phase to SSH and SST and Ta parameters (Figure 3e). Anomaly positive of chl-a during the SEM is coincident with negative anomaly of temperature and SSH anomaly. This may be related to upwelled nutrients- rich water from deeper layer to surface layer stimulate phytoplankton growth that increase chl-a concentration.

Seasonal Variation of Wind-stress, Seas Surface Temperature and Chlorophyll-a

Monthly averaged surface wind-stress, SST and Chl-a in February and September 2017 are shown in Figure 4, 5 and 6. In September (as a representative of the peak of SEM period) the southeasterly wind field vectors were much stronger than that the northwesterly

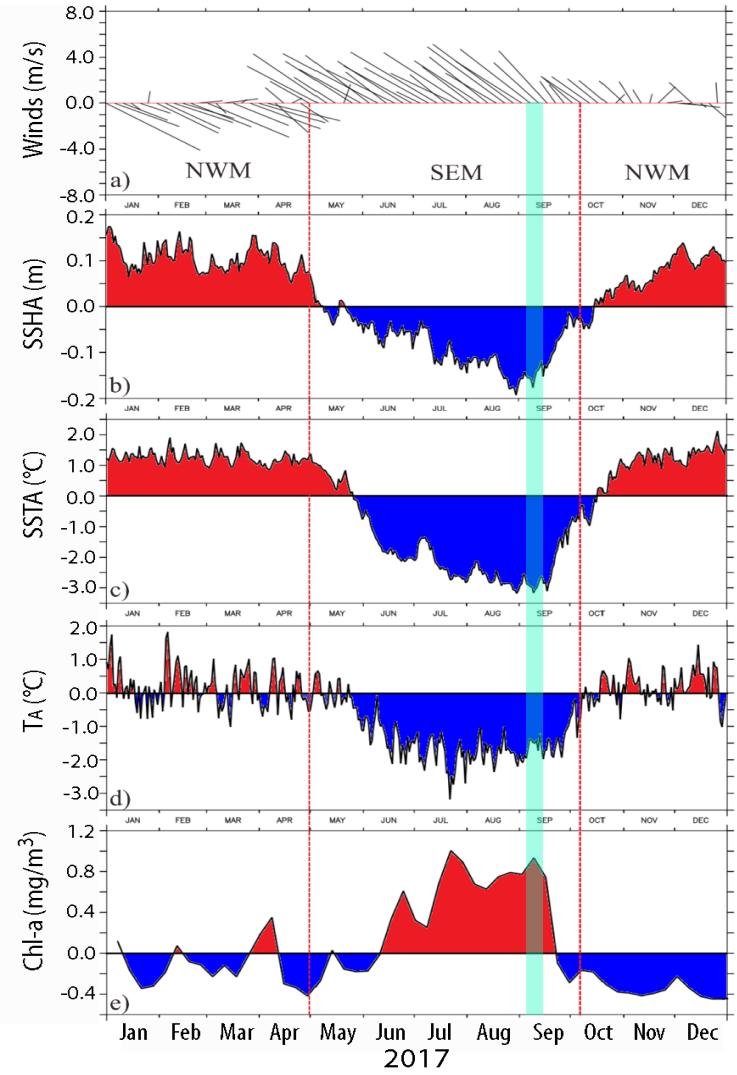

Figure 3. Time series of surface ocean-atmosphere parameters, averaged from a dashed black rectangle in Figure 1; (a) surface winds vectors; (b) anomaly of SSH; (c) anomaly of SST; (d) anomaly of air temperature; and (e) anomaly of surface chl-a in 2017. Vertical cyan-line denotes for field measurement time from 2 to 12 September 2017.

monsoon winds vectors in February (during the NWM period) (Figure 4a). Magnitude of wind-stress in 2017 in the northern Arafura Sea varied between 0.01 - 0.18 Pa with average of 0.06(±0.013) Pa. Maximum wind-stress vectors during the NWM appeared in February with average winds speed is 6.11 m/s. During the SEM period, maximum wind stress was found in June with wind speed of 8.23 m/s. However, on the climatology mean

the maximum of wind-stress occurs in August (Sprintall & Liu, 2005). The southeasterly wind fields are fully developed in central Arafura Sea with magnitude of wind-stress were much stronger during the SEM than that during the NWM. In particular, the maximum of wind-stress field in September 2017 exhibited around southern peninsula of Digul Papua (Figure 4b).

Seasonal upwelling event was examined from evolution of satellite-derived sea surface temperature (SST) and surface chl-a in 2017, since we had field CTD measurement in September 2017. Here, we contrasted spatial distribution of monthly mean SST and chl-a during the NWM period (February 2017) and during the SEM period (September 2017) (Figure 5).

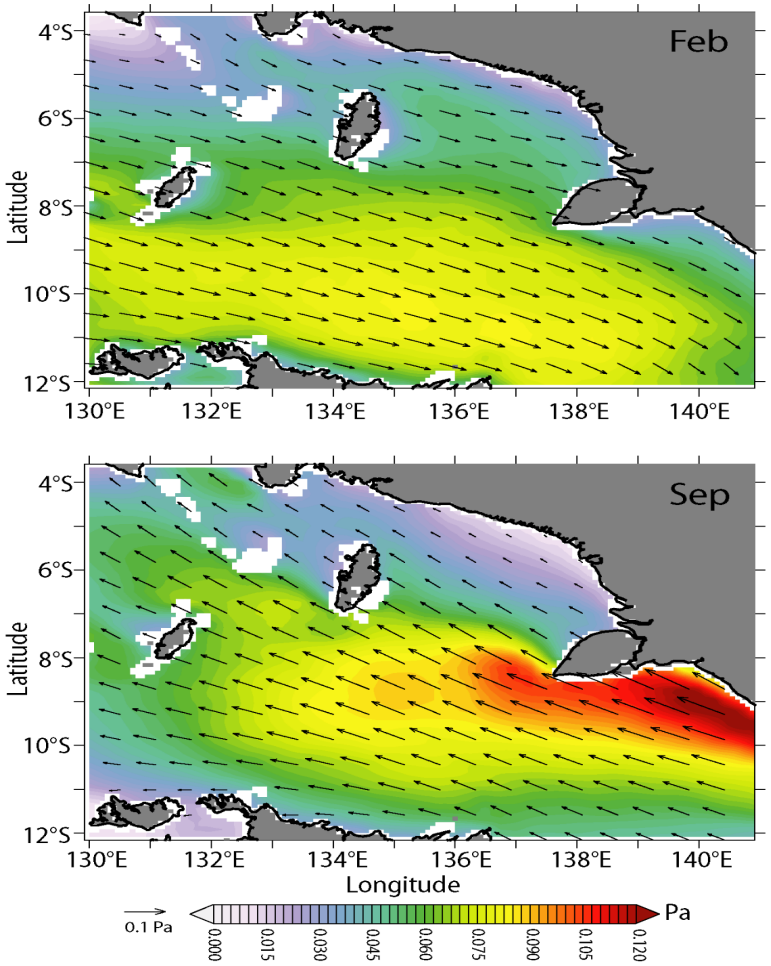

Figure 4. Monthly average of wind-stress vectors. Color denotes wind-stress magnitude in the study area for February (upper) and September 2017 (lower)

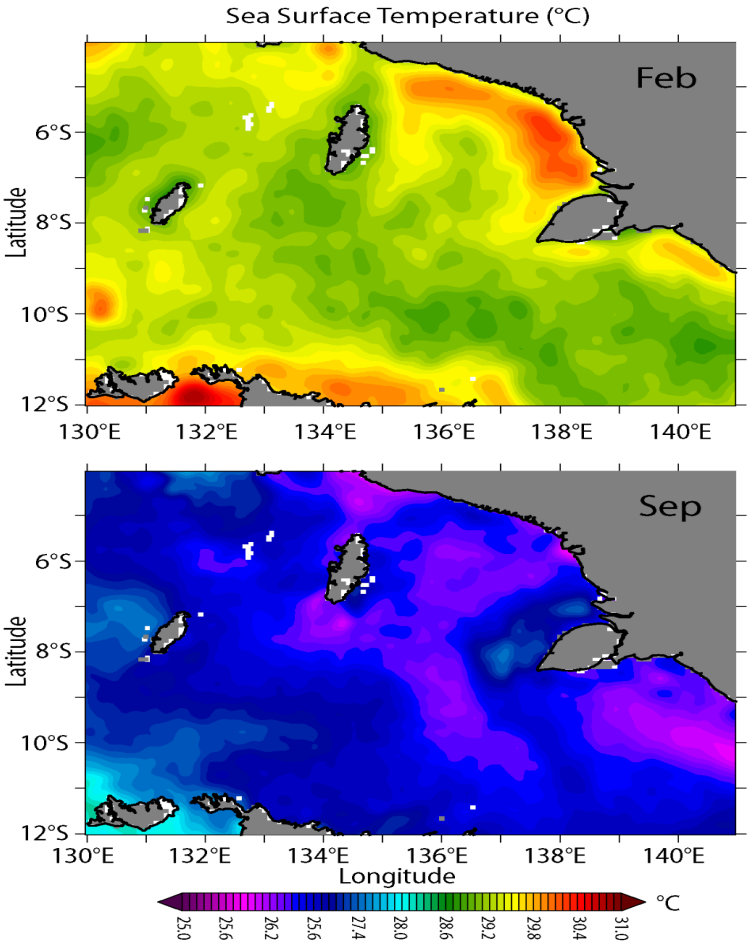

Figure 5. Monthly average of satellite-derived sea surface temperature (SST) in February (upper panel) and September 2017 (lower panel)

Distribution of monthly average SST in the study area in 2017 varied between 24.1 - 33.0°C with mean SST of 28.7(±1.5)°C. Seasonal changes of solar radiations and upwelling processes contribute to this large SST variation in this region (Gordon & Susanto, 2001; Condie, 2011; Kida & Richards, 2009;). During the SEM period, SST was much colder since heat budget from solar radiation was surplus in northern hemisphere. In contrast, during the NWM period, when southern hemisphere was surplus of heat budget, warmer SST was found (Figure 5). Furthermore, during the SEM period the southeasterly winds were much stronger than that during the NWM period. The SEM winds have also a significant spatial variation with strongest winds over the southeastern Banda that create upwelling (Condie, 2011; Kämpf, 2015).

During the NWM (February) the SST varied between 28.4 and 33.1°C with mean SST of 30.1(±0.6)°C. Much warmer SST was found around Aru Islands and northern Arafura, southwest Arafura, and around Digul Peninsula (Figure 3). In February 2017, SST ranged between 28.4 and 31.6°C. An increased temperature was found in March 2017 (28.7-31.7°C) and commenced to decrease in April and May 2017 with SST varied 27.5-31.1°C and 27.0-31.1°C, respectively. This SST variation is consistent with past studies (Dewi et al., 2018).

During the 2017 SEM period (September), SST varied between 24.3-29.8 °C with mean value of 27.0 °C. It shows that development of colder water is derived from southwestern coastal area of Papua. This colder water is commenced from May to September (Figure 3). In northern Arafura (around Aru island), evolution of colder SST appeared from June to October indicated by a patch of colder temperature of about 27.0°C which gradually grew much cooler and larger area and reached its minimum of 24.0°C in September. Extension of colder water distribution decreased in September and near the coastal Papua region colder temperature of 24.1°C was present. After that, SST commenced to increase in October 2017 with an increase temperature of 1.8°C. Here, temperature varied between 26.2 and 31.9°C. In November 2017 SST varied between 27.9 and 32.4°C (Figure 3).

Figure 6 shows a contrast of surface chl-a during the NWM (February) and SEM (September) in Arafura Sea. It is seen clearly a high chl-a in coastal area of the northern Arafura Sea both during different monsoon period. However, in the SEM period, high chl-a extended to the west between Aru and peninsula of Digul Papua.

In 2017 surface chl-a concentration in the study area varied between 0.02 - 12.85 mg/m^3 with average of 0.53(±0.89) mg/m^3. In the coastal waters of the northern Arafura Sea surface chl-a is always high around the year. This may be related to high contribution of rivers discharge from many rivers in Papua (Kämpf & Chapman, 2016). Mean surface chl-a (in 2017) during the NWM period was lower than that during the SEM period (Figure 6).

Distribution of surface chl-a during the NWM period (February) ranged between 0.02 and 6.53 mg.m-3 with mean value of 0.31(±0.61) mg/m^3 (Figure 6). In Arafura Sea during this period precipitation rate exceeds evaporation rate (Wyrtki, 1961). Thus, high nutrient inflow from river discharge into the coastal waters influence significantly on high chl-a concentration near the coastal area. Monthly mean of surface chl-a increased gradually from May with chl-a concentration of 0.57 mg/m^3. A drastic increase of surface chl-a was revealed during the SEM period that varied between 0.02 and 12.85 mg/m^3 with mean value of 0.98(±1.11) mg/m^3.

Surface chl-a reaches its maximum in the peak of SEM period (July-August-September). According to Kämpf (2016), spatial distribution of chl-a between June and October increases significantly, where horizontal distribution of chl-a extends to area of

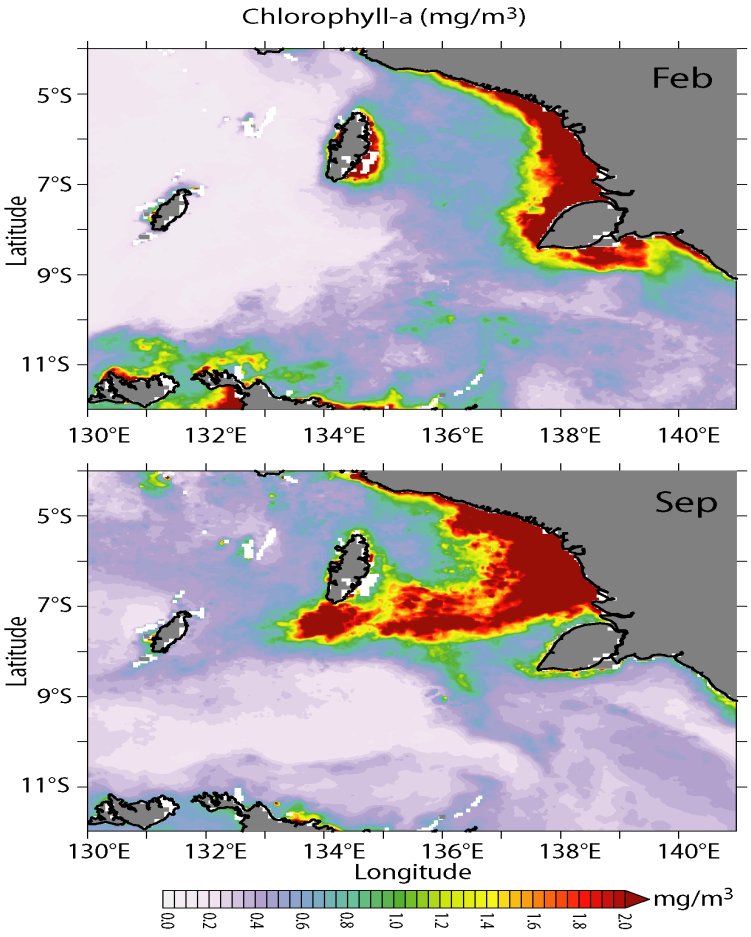

Figure 6. Monthly average of satellite derived surface chl-a in February (upper panel) and September 2017 (lower panel)

about 90,000 km^2. Starting from October, concentration of chl-a decreased again to about 0.33 mg/m^3, and this trend continued decreasing in December to about 0.15 mg/m^3.

This maximum surface chl-a concentration which is related to minimum SST during the SEM period may corroborate upwelling event. In contrast, during the NWM period maximum SST is followed by minimum of chl-a concentration. Upwelling process may contribute to that out-of-phase fluctuation between surface chl-a and SST, in which during the upwelling event colder and nutrients-rich deeper water mass is lifted up to near-surface layer. The availability of this unique water mass is utilized by phytoplankton in photosynthetic process, so that a drastic growth of phytoplankton is evident (Taufikurahman & Hidayat, 2017).

Stratification of Water Mass During Upwelling Event

Profiles of temperature, salinity and potential density anomaly (hereafter referred to as the parameters) in 3 CTD stations in section A (Figure 7a) revealed a step-like pattern with two strong vertical gradients of parameters in the upper 7 m (0.08-0.22°C m^{-1}), and between 31-35 m depth (0.10-0.18°C/m). In-between, a homogeneous layer was found between 7-30 m and 35-70 m depth. Step-like profiles may be formed due to different surface winds. The homogeneous layers at the beginning may be created by strong surface winds that mix surface layer. These conditions take place continuously, but the strength of the wind may vary and weaken causing the formation of this stratification (Tomczak, 2014). Other factor may be related to different flows direction in the sub-surface and near-bottom flow, as suggested by Kämpf (2015) where near-bottom flow directed eastward and westward flow in near-surface layer.

Spatial variation of temperature in the upper 30 m depth from station 1 to 3 was also seen, where colder water was found in station 3 (green) close to coastal area, and temperature at station 1 was much colder than station 2 at depth between 35 and 55 m depth. Salinity profiles showed a small variation and very fresh water in the upper 5 m depth. Density anomaly profiles are controlled strongly from temperature profiles.

Transect A was closed to coastal area (Figure 7b), so the upwelling process is expected much stronger compared to other two sections B and C. Here, slope from offshore to coastal area of isotherm of 25°C, isohaline of 34.25 psu, and isopycnal of 22.75 75 kg/m^3 from about 30 m depth to the sub-surface (about 5-10 m depth) were seen clearly. Strong vertical stratification in the upper 10 m was also observed as shown with plenty contours of parameters. Near surface layer temperature was about 26.5°C.

Profiles of the parameters in section B formed a step-like structure with different mixed homogeneous layers depth for each station (Figure 8a). For example, at station 4 offshore area (grey profiles), a homogeneous temperature was found in the upper 28 m depth, then from 29 m to 40 m depth a high vertical gradient of temperature of 0.19°C/m was seen before the second homogeneous layer.

Consistently, a cross-section of temperature-salinity and potential density anomaly in transect B (this is the longest section, about 150 km from offshore to the coastal area) revealed a clear signature of shallowing contours of these parameters from offshore to near coastal waters. Here, isotherm contours of 25.0°C and 25.5°C at depth near 40 m in the offshore area (as well as isohaline contours of 33.75 psu, 34 psu, and 34.25 psu; and isopycnal contours of 22.75 kg/m^3, 22.5 kg/m^3, and 22.25 kg/m^3) were uplifted to shallower depth of 5-10 m depth (Figure 8b). A very freshwater (<32.5 psu) and less density water surface layer water were found only in station 7, which might be related to runoff from rivers in the region. The shallowing isotherm, isohaline, and isopycnal contours from deeper layer in offshore toward the coastal waters indicated an upwelled water as a response on

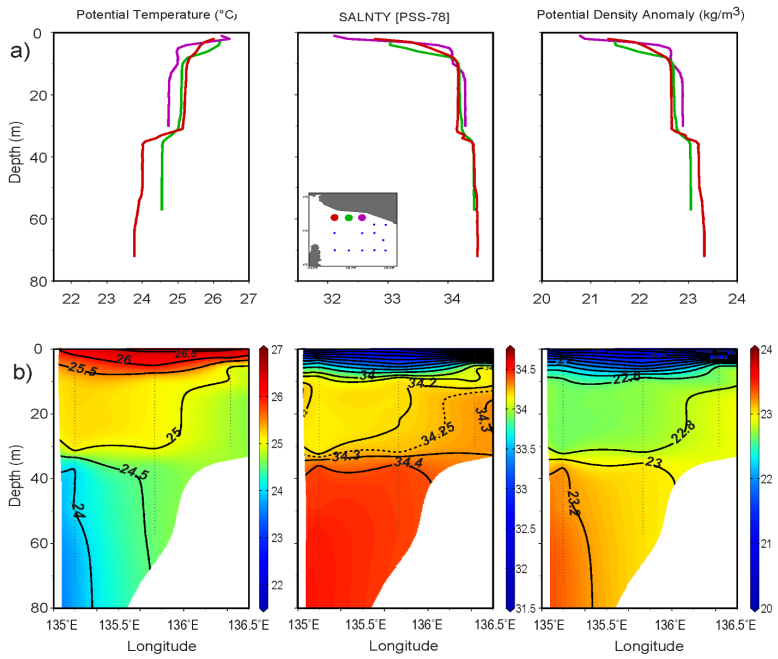

Figure 7. Profile of parameters (a) and its depth-longitude distribution (b) in section A

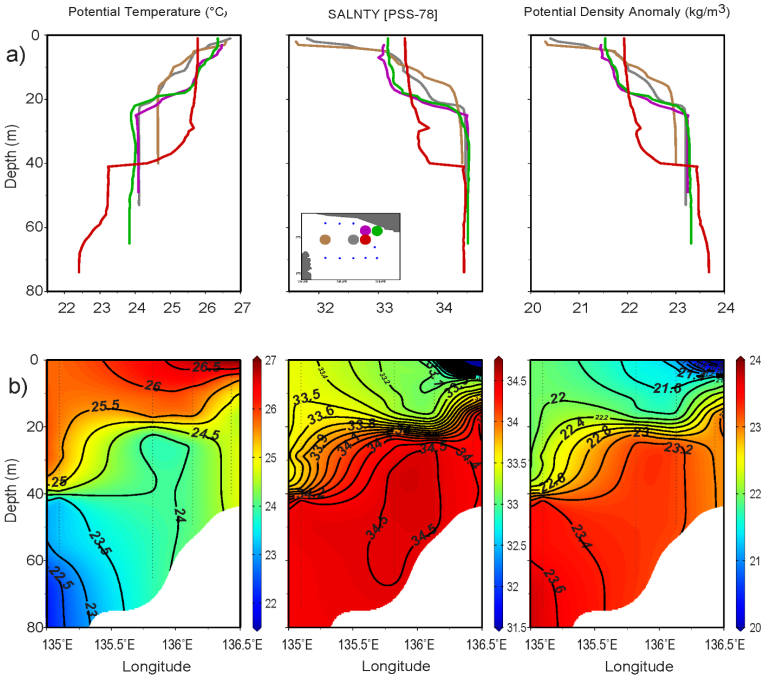

Figure 8. Profile of parameters (a) and its depth-longitude distribution (b) in section B

surface Ekman transport that brought near surface water away from coastal area, and then deeper water filled these surface water. This implies that there should be present near-bottom flow eastward that contrast to those in near-surface layer. Indeed, this reversal flows are found from the model current which will be discussed later in next section (Figure 13b).

Vertical profiles of the parameters at stations in section C showed a similar pattern (except for profile at station 7) with first homogeneous layer in the upper 20-25 m depth, then strong vertical gradient of temperature (0.36 – 0.45°C/m between 23-29 m depth, and then second homogeneous layer below 23 – 29 m depth to the bottom (Figure 9a). Vertical profile at station 7 revealed high vertical gradient of 0.15 in the upper 16 m depth, and a homogeneous layer below that.

In Transect C, shallowing of contours of isotherm, isohaline and isopycnal was also seen, but it lessened from 30 m to 20 m depth (Figure 9b). However, contour of isotherm 26°C extended from surface to about 20 m depth, as well as isohaline contour of 33 psu, and isopycnal of 22.0 kg/m^3. It is also shown an outcropping of isohaline 33.25 psu and isopycnal 21.75 kg/m^3 from 25 m depth in the offshore region to surface near the coast.

Vertical profile and stratification of the parameters in three CTD sections showed an evidence of upwelling processes in the study area, where colder, saltier and heavier water from deeper layer (30-40 m depth) in the offshore area were consistently uplifted toward the shallow coastal area. Here, upwelling indicator from CTD datasets could be defined for isotherm between 25.5 and 26.0°C, isohaline of 33.5-33.75 psu, and 22.5-22.75 kg/m^3. Surfacing of these parameters varied spatially, for example, these contours appeared in the upper 5 m, 9 m, and 20 m in the section A, B, and C, respectively.

Temperature-salinity relationship exhibits a structure of upwelling coastal water mass with the deepest CTD measurement of approximately 80 m depth. This may represent upper-thermocline water derived from adjacent deep Aru basin (Figure 10). Salinity varied from 31.62 psu at surface layer to 34.63 psu at deeper layer with mean salinity of 33.955 psu (±0.605). Potential temperature ranged from 21.995 °C to 26.707 °C with mean temperature of 24.559°C (±1.131), and potential density anomaly from 20 to 24 kg/m^3. Very fresh surface water was found at the stations closed to the coastal waters, but salty water was found at stations in the offshore and central area. Water mass with salinity maximum (34.6 psu) was found at surface density between 23.0 and 23.5 kg/m^3 which represented upper thermocline water. Relatively salty water (>34.0 psu) was found at approximately 40 m depth at the offshore but was uplifted to about 20 m depth in the onshore area. This spatial variation of seawater properties between shelf-break and inner-shelf regions may be associated with upwelling process. Mechanism of this coastal upwelling is discussed in the following section.

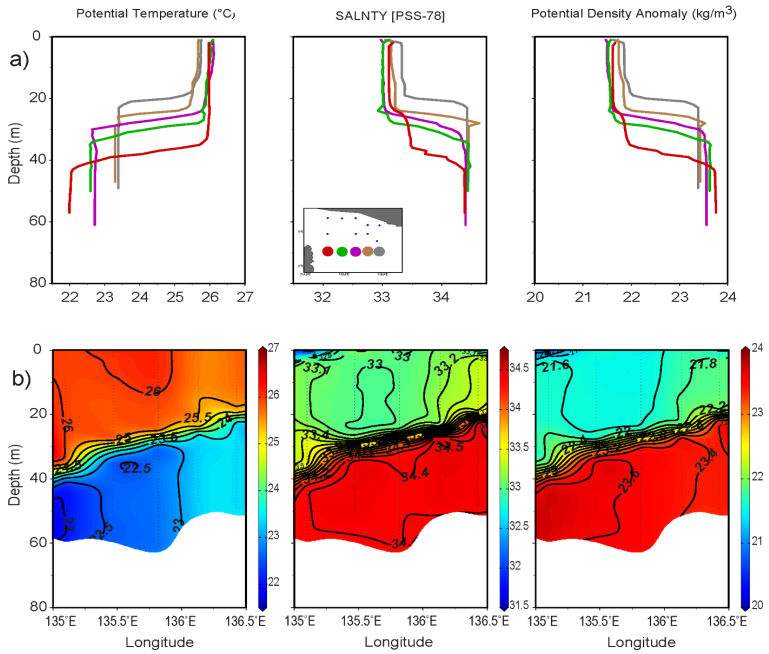

Figure 9. Profile of parameters (a) and its depth-longitude distribution (b) in section C

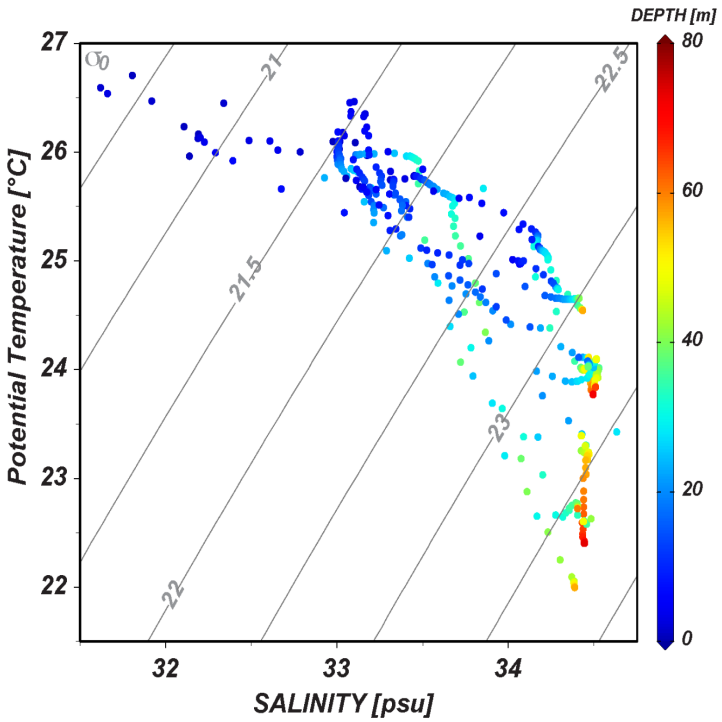

Figure 10. Temperature-salinity relationship (T-S diagram) plotted from 13 CTD casts during the Geomarine 3 cruise on 2-12 September 2017 in the northern Arafura Sea

Upwelling Mechanism in the Northern Arafura Sea

Previous analysis from derived-satellite parameters and field measurement datasets have demonstrated a strong indication of upwelling event. Here we proposed, a classical theory of coastal Ekman upwelling, as a physical mechanism of generating upwelling forced by the SEM winds field. Then, we evaluate regional circulation which may modulate the Ekman upwelling dynamics.

The strong persistently southeasterly monsoon winds during the SEM period which are fully developed from May to November are considered to be a main generating forcing of coastal upwelling in Arafura Sea (Figure 4). By applying Ekman upwelling theory, during the SEM period strong persistent southeasterly winds drive surface current westward-northwestward (or 45° from wind direction to the left) and integrated Ekman transport from surface to Ekman depth is expected drifting southwestward from wind direction which is away from the coastline of Papua. The continuity implies that transported surface water offshore must be replaced by water from deeper layer, and the upwelled water must be created. On the other hand, wind-stress fields in February 2017 may lead to generate downwelling since the Ekman drift directed to the coastal waters. The southeasterly (northwesterly) wind-driven surface current in the study area can be inferred from the surface and subsurface current field during different monsoon peaks, as discussed below.

Model surface current vectors at two depth levels (5 m and 25 m) overlaid with model temperature in February (the peak of NWM period) and September 2017 (the peak of SEM period) revealed a contrast of surface and subsurface flows pattern (Figure 11a-b). In February, circulation in the northern Arafura Sea, adjacent Aru island (north of 8°S), exhibited warm water and revealed two anti-clockwise eddies in northern and western Aru (Figure 11a). Relatively strong current vectors from Banda Sea and northern Aru basin flowed eastward into northern and southern Aru, which was consistent at 5 m and 25 m depths. In the Arafura shelf, surface circulation at 5 m depth during this period tends to flow eastward, but it is slightly different at 25 m depth, particularly along northern coastal water where weak northwestward flows are found.

During the SEM period (in September), a contrast of surface and subsurface circulation was seen (Figure 11b). At 5 m depth level, strong current vectors from Aru basin flow southeastward and deflected westward into Banda Sea in west of Aru. Furthermore, a relatively strong current vector that brought colder water from northern Aru flow westward which then join with current from Aru basin into Banda Sea. The westward flowed at this 5 m depth level appeared mostly over the region, such as at around latitude band of 7°S – 10°S (Figure 11b). As expected from Ekman upwelling theory, during the SEM period, surface current flows generally westward away from the coastal waters, as a response to the persistent southeasterly monsoon winds (Figure 4). Here, the minimum SST of 26°C appeared in September with much colder water occurring near northeastern Aru.

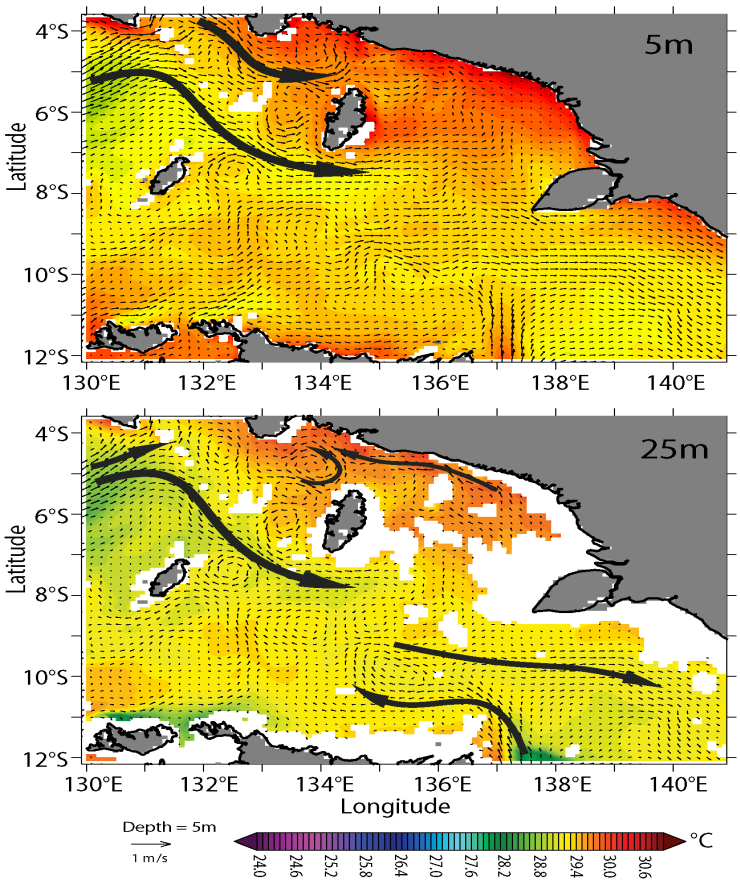

Figure 11a. Model surface current vectors, overlaid with model sea surface temperature at 5 m and 25 m depth in February 2017

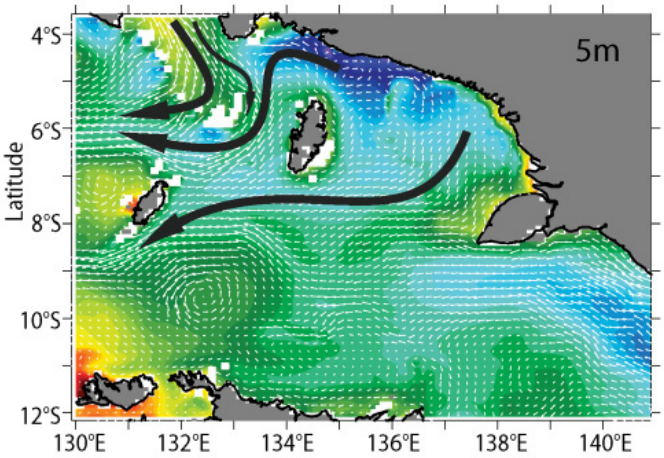

Figure 11b. Model surface current vectors, overlaid with model sea surface temperature at 5 m and 25 m depth in September 2017

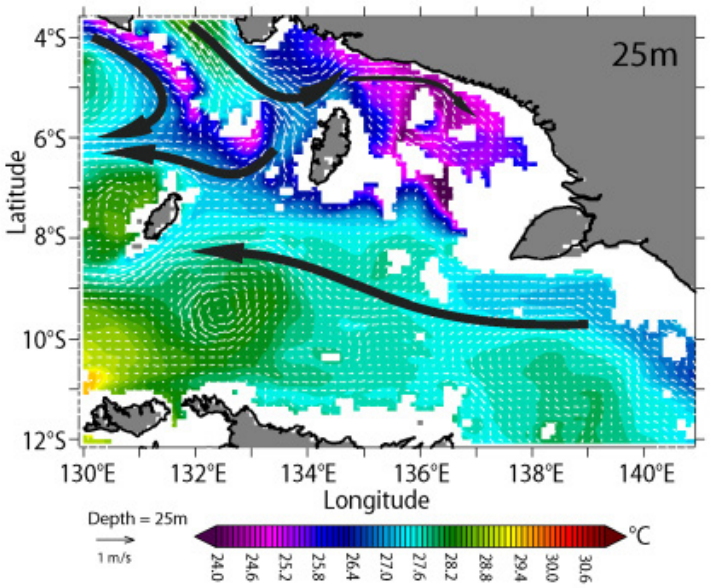

Figure 11b. (Continued)

Nevertheless, at 25 m depth to the deeper layer, reversed current vectors were found in the northern Aru island, where much stronger southeastward currents from Aru basin entered the Arafura shelf-slope (between Aru and Papua), and flowed eastward into the shelf, and the remaining flow southward and deflected westward into Banda Sea (Figure 11b). Here, a contrast of circulation was found: westward flow in surface layer that bring surface water away from coastal waters, and eastward inflow below subsurface that bring Aru basin water into the shelf waters. This strong southward Aru basin inflow may depict regional circulation of the Indonesian Throughflow (ITF) from Halmahera Sea that flows along outer Banda Arcs and enters into the study area (Masoleh &Atmadipoera, 2018). Trajectory analysis of water particles from Halmahera Sea confirmed the pathways of strong seasonal flow from Halmahera along outer Banda arcs during the SEM period (Wattimena, 2020). Thus, the presence of strong subsurface Banda arcs - ITF inflow into the Arafura shelf-break between Aru and Papua at 134°E can supply colder, saltier and nutrient-rich water and modulate the intensity of Ekman upwelling there. Kämpf (2015; 2016) suggested that this inflow was derived from Banda sea slope water since the model domain covered only eastern part of Banda Sea constrained to 132°E in the west and to 4°S in the north.

Schematic upwelling processes during the SEM period in the study area is presented in Figure 12. Much stronger southeasterly winds during the SEM period is associated with much stronger magnitude of surface current speeds. Susanto et al. (2001) suggested

that the monsoonal winds were the main forcing for generating coastal upwelling. Here, along-shore southeasterly winds generate surface current deflected about 45° to the left due to Coriolis effect from the wind direction (about westward). Below surface layer current directions are also deflected consecutively until the Ekman depth layer, forming the Ekman spiral. If we integrated this flow from surface to Ekman depth, then we have Ekman transport (Et) flowing southwestward or away from the coastal water (Figure12a). This creates horizontal pressure gradient between offshore and coastal waters, indicating by low sea surface height and reducing coastal water mass which is restored by upwelling water from deeper layer (Figure12b). Thus, surface Ekman transport flowing offshore generates upwelled deeper water in the coastal waters (Stewart, 2006).

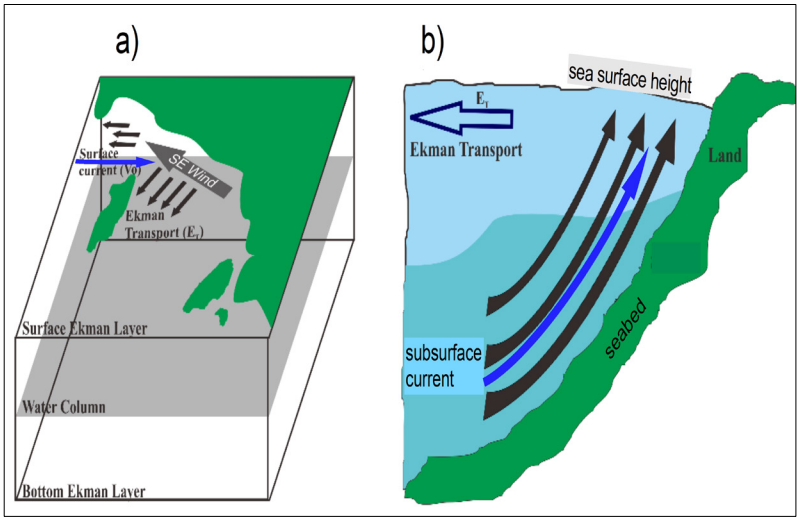

Figure 12. Schematic upwelling processes in the study area, (a) 3-dimension landscape figure; and (b) schematic cross-section in water column

In particular, in northern Arafura shelf sea, upwelling dynamics is not only controlled by the southeasterly winds that generate Ekman upwelling as described above, but also may be modulated by the subsurface current that inflows from the shelf-break into the inner shelf waters. Regional current system along the outer Banda arcs as a branch current of Indonesian throughflow (ITF) may contribute significantly on the upwelling process which then modulate intensity of upwelling. The presence of outer Banda arcs current – ITF may favor the upwelling intensity during the SEM period.

Further analysis on this subsurface deeper layer from a depth-latitude between Aru and Papua at 134.25 °E (please refer to yellow-line in Figure 1), revealed a reversed current

between surface and subsurface layer (Figure 13). During different monsoon period the core of strong eastward inflow into Arafura shelf slope appeared much stronger and larger from subsurface (20 m depth) to approximately 100 m depth during the SEM period than that during the NWM period from surface to about 50 m depth (Figure 13a). The westward flow in the upper 25 m was seen clearly during the SEM period. This current was a direct response to the southeasterly winds. At least, in the mid-section to the south the eastward flow was present during both monsoon periods, but the eastward flow during the 'SEM' upwelling period played a significant role to modulate upwelling dynamics by charging drifted surface water of Ekman transport.

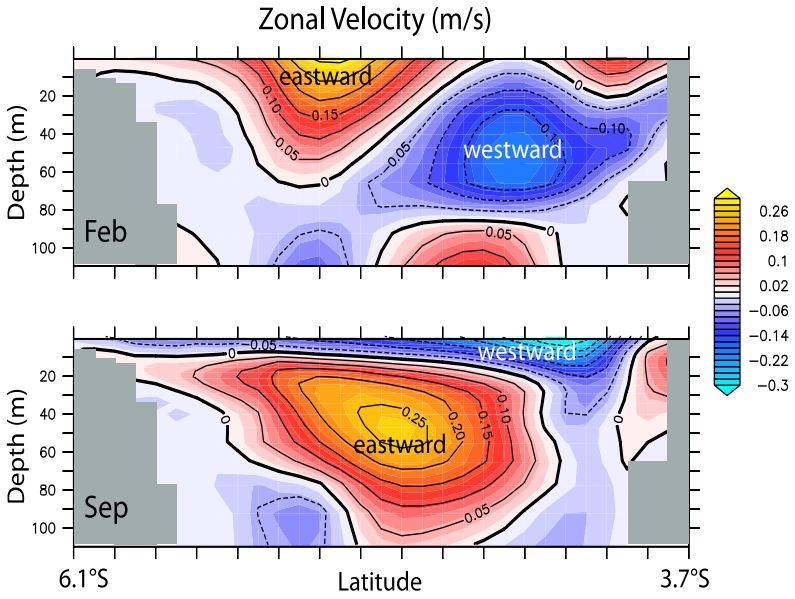

Figure 13a. Cross-section of model zonal current component in (a) February, and (b) September 2017. (Please refer to yellow line in Figure 1)

Furthermore, a depth-longitude plot of model zonal current component in the study area (please refer to red-line in Figure 1) shown in Figure 13b, exhibits the upwelling processes during the SEM period (September) as described above. Surface current flowed westward or away from coastline, while subsurface shelf-break current below 20 m depth to the bottom flows eastward that supplied colder, saltier and nutrient-rich water from deeper layer to the upwelling area (Figure 13b). This is contrast to the NWM period (February) when the surface current flowed eastward, accumulating surface water in coastal area, and created subsurface current flowing westward (Figure 13a).

This zonal current pattern in September 2017 is in good agreement with cross-section of temperature, salinity and potential density anomaly (Figure 7-9), in which subsurface eastward shelf-break flow (Figure 13b, in Sep) is associated with a homogeneous water mass in the second mixed layer or below the barrier layer with sharp stratification of uplifting isotherm of 25°C, isohaline of 34 psu and isopycnal of 22.5 kg/m^3 from deeper layer (30-40 m depth) at shelf-break area to near-surface layer (10 m) in the inner shelf area. This subsurface eastward flow has been also discussed by Kämpf (2015; 2016), suggesting that this existence of undercurrent-driven upwelling below 20-30 m depth was derived from Banda slope water. We found that this eastward inflow was as a branch current originated from the outer Banda arcs current flowing from Halmahera Sea into eastern Seram Sea and flowed along outer Banda arcs and entered northern Arafura shelf sea, as part of the ITF.

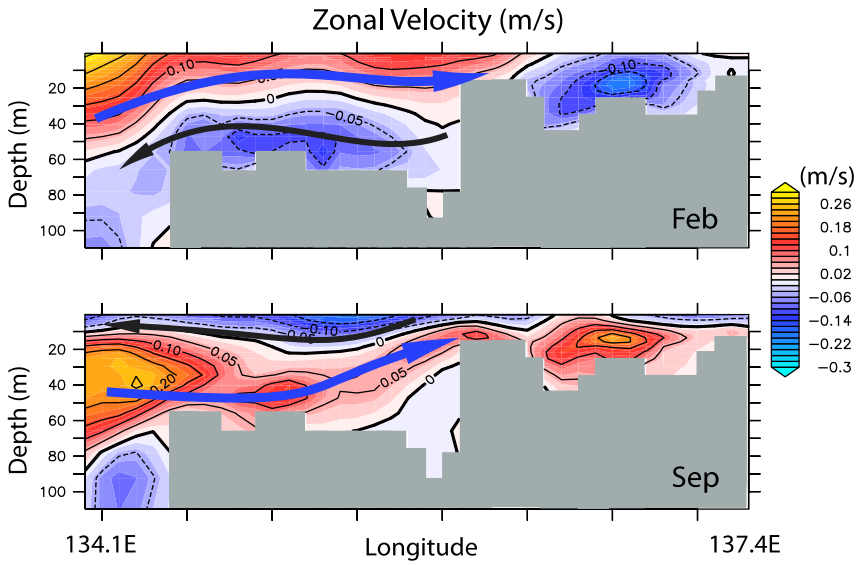

Figure 13b. Cross-section of model zonal current component in (a) February, and (b) September 2017. (Please refer to red line in Figure 1)

Estimates of Transport Volume in the Upwelling Region

In this study, two methods had been applied to calculate transport volume for quantifying Ekman transport, near-surface, and subsurface transports due to upwelling: by using classical "atmospheric" methods which is based on wind-stress calculation at a particular section, and by using "ocean" method, based on integrating of model zonal current component at a meridional section.

Monthly average of Ekman transport (TE) was calculated from wind stress data along a section (please refer to green-line in Figure1) to quantity of transported water mass away from coastline during upwelling event or toward coastline (downwelling period). It is found that from December to April (during the NWM period) the positive Ekman transport was toward the coastal area, which is associated with downwelling process, with maximum transport in February (0.46 Sv) (Figure 14). On contrary, negative Ekman transport (toward offshore) was revealed from May to November during the SEM period (upwelling period) with maximum transport to offshore in June (-0.71 Sv) (Figure 14). Negative Ekman transport was associated with coastal upwelling event from May to November, which is consistent with previous discussion (Wyrtki, 1961). As described in the method, Ekman transport estimate is sensitive to the wind-stress datasets. For example, wind-stress series is maximum in June 2017 which is related to the maximum of Ekman transport in June 2017 (Figure 14)

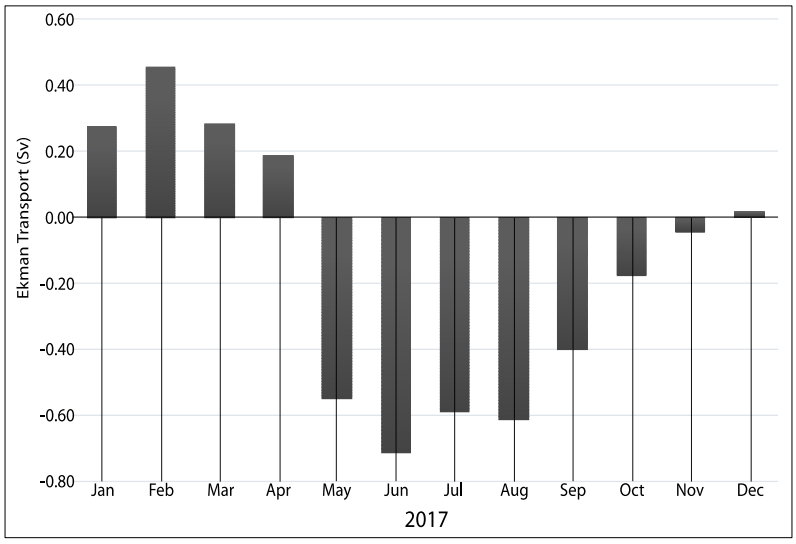

Figure 14. Monthly average of Ekman transport in coastal upwelling region in 2017 (please refer to green line in Figure 1)

Transport volume is also estimated from integration of zonal current component from the ocean circulation model which has been configured with both atmospheric and oceanic forcing in the model. Here, based on monthly average of zonal current in September 2017 (Figure 13a), we calculated transport volume at three layers (0-25m, 25-55m, and 55-110m). As expected, in the first layer (0-25 m depth) during the upwelling period a westward transport was seen clearly from May to end of September 2017 with its mean transport of -0.28 (±0.34) Sv (westward) and its transport maximum of -0.899 Sv at the end of August

- early of September (Figure 15). At second layer (25-55 m depth) the mean transport volume during the SEM period was +0.65 (±0.19) Sv (eastward), and at third layer (55-110 m depth) the mean transport was +0.41 (±0.213) Sv (eastward). The mean transport from 25 m to 110 m depth was +1.06 (±0.29) Sv. This implies that an inflow from Aru basin into the shelf waters during the SEM period may regulate the Ekman upwelling and also supply Arafura shelf sea with much colder, saltier and nutrient-rich water originated from deeper outer Banda arcs throughflow.

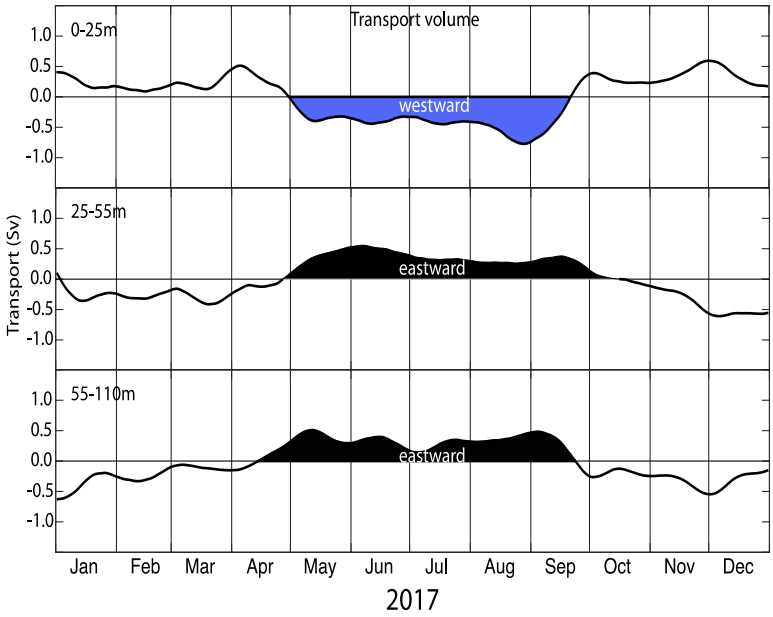

Figure 15. Daily transport volume series, integrated from 25m to sea surface (upper panel), from 55 m to 25 m depth (middle panel), and from 110 m to 55 m depth (lower panel) (please refer to yellow line in Figure 1). The transport volume time-series are smoothed with 15-day cut-off.

CONCLUSION

Physical processes and dynamics of upwelling in the northern Arafura Sea in 2017 had been investigated, by using multi-datasets from CTD casts, satellite-derived parameters, and validated ocean circulation model outputs. The evidence of upwelling clearly observed from a sharp barrier layer separating first mixed layer from second homogeneous layer beneath subsurface layer. This barrier layer formed large upsloping isotherms of 23.5 - 25.5°C, isohalines of 33.5 - 34.25 psu, and 21.8 - 23.2 kg/m^3 from deeper layer (30-40 m depth) in the shelf-break area to subsurface layer in the inner shelf waters, where much

colder and saltier water occured in shallower depth. A homogeneous water in the upper-layer is related to Ekman upwelling drift that is generated by the southeasterly monsoon winds, but the second homogeneous water beneath the barrier layer is belong to a distinct water mass which may be originated from the deeper shelf-break area. The existence of two mixed layer separated by the barrier layer corroborates a reversed current direction, where upper-layer current flowing westward – away from the shelf and strong subsurface current flowing eastward into the shelf. Therefore, the upwelling dynamics here is generated mainly by the persistent southeasterly winds leading to Ekman drift westward in the upper-layer, and is modulated by the subsurface eastward current from deeper shelf-break into the inner-shelf. The latter is not local current but a regional current which is considered derived from the outer Banda arcs current system as a current branch of the Indonesian Throughflow. Mean transport volume in the upper layer (0-25 m depth) between Aru and Papua during upwelling period (May – September) was -0.28 (±0.34) Sv (westward), and transport between 25m - 110m was +1.06 (±0.29) Sv (eastward), suggesting this inflow may regulate the upwelling and supply colder, saltier, and nutrient-rich water into Arafura shelf water. Transport volume derived from wind-stress calculation revealed its maximum in June, which is different from the ocean current calculation from May to September and its maximum in August-September. Surface ocean parameters reveal that onset (termination) of upwelling in May (October) is indicated by the reversed southeasterly winds, negative anomaly of SST, SSH, air temperature, but positive anomaly of chlorophyll-a.

ACKNOWLEDGEMENTS

The authors express their gratitude to the captain and the crews of Research Vessel GEOMARIN 3 for professional works and helps during field experiment. We also thank H. Catur Widiatmoko, MSc., team leader, for an excellent onboard coordination. Satellite derived sea surface temperature and surface chlorophyll-a dataset were obtained from Mercator Ocean/ Copernicus, available at (https://www.marine.copernicus.eu). Ocean general circulation model output datasets performed by CLS Toulouse France and were obtained from INDESO, available at (https://www.indeso.go.id). Surface meteorological datasets were obtained from the ECMWF, available at (https://www.apps.ecmwf.int). The Author also thank to the reviewers who gave a constructive criticism for the paper improvement.

REFERENCES

Alongi, D., Edyvane, K., do Ceu Guterres, M., Pranowo, W., Wirasantosa, S., & Wasson, R. (2011). *Biophysical profile of the Arafura and Timor Seas.* Jakarta, Indonesia: Arafura and Timor Seas Ecosystem Action (ATSEA) Program.

Atmadipoera, A.S., Khairunnisa, Z., & Kusuma, D. W. (2018). Upwelling characteristics during El Nino 2015 in Maluku Sea. *IOP Conference Series: Earth and Environmental Science, 176*(1), 1-18.

Atmadipoera, A. S., & Widyastuti, P. (2015). A numerical modeling study on upwelling mechanism in Southern Makassar Strait. *Jurnal Ilmu dan Teknologi Kelautan Tropis, 6*(2), 355-371.

Condie, S. A. (2011). Modeling seasonal circulation, upwelling and tidal mixing in the Arafura and Timor Seas. *Continental Shelf Research, 31*(14), 1427-1436.

Copernicus Marine Service. (2019). *Product user manual for all ocean colour products.* Retrieved June 18, 2020, from https://resources.marine.copernicus.eu/documents/PUM/CMEMS-OC-PUM-009-CHL-A.pdf

Dewi, D. M. P. R., Fatmasari, D., Kurniawan, A., & Munandar, M. A. (2018). The impact of ENSO on regional chlorophyll-a anomaly in the Arafura Sea. *IOP Conference Series: Earth and Environmental Science, 139*(1), 1-18.

Emery, W. J., & Thomson, R. E. (2004). *Data analysis methods in physical oceanography.* Massachusetts, USA: Elsevier.

Garnesson, P., Mangin, A., d'Andon, O. F., Demaria, J., & Bretagnon, M. (2019). The CMEMS GlobColour chlorophyll a product based on satellite observation: multi-sensor merging and flagging strategies. *Ocean Science, 15*(3), 819-830.

Gordon, A. L., & Susanto, R. D. (2001). Banda sea surface-layer divergence. *Ocean Dynamics, 52*(3), 0002-0010.

Kämpf, J. (2015). Undercurrent-driven upwelling in the northwestern Arafura Sea. *Geophysical Research Letters, 42,* 9362-9368.

Kämpf, J. (2016). On the majestic seasonal upwelling system of the Arafura Sea. *Journal of Geophysical Research Oceans, 121,* 1218-1228.

Kämpf, J., & Chapman, P. (2016). *Upwelling systems of the world: A Scientific journey to the most productive marine ecosystems.* Berlin, Germany: Springer International Publishing.

Kida, S., & Wijffels, S. (2012). The impact of the Indonesian throughflow and tidal mixing on the summertime sea surface temperature in the western Indonesian Seas. *Journal of Geophysical Research: Oceans, 117*(9), 1-14.

Kida, S., & Richards, K. J. (2009). Seasonal sea surface temperature variability in the Indonesian seas. *Journal of Geophysical Research Oceans, 114*(C6), 1-17.

Kutsuwada, K. (1998). Impact of wind/wind-stress field in the North Pacific constructed by ADEOS/NSCAT data. *Journal of Oceanography, 54*(5), 443-456.

Masoleh, V.C., & Atmadipoera, A.S. (2018). Coherence of transport variability along the outer Banda arcs. *IOP Conference Series: Earth and Environmental Science, 176,* 1-13.

Pond, S., & Pickard, G.L. (1983). *Introductory dynamical oceanography.* Massachusetts, USA: Elsevier Butterworth-Heinemann.

Rosdiana, A., Prartono, T., Atmadipoera, A. S., & Zuraida, R. (2017). Nutrient and chlorophyll - A distribution in Makassar upwelling region: From MAJAFLOX cruise 2015. *IOP Conference Series: Earth and Environmental Science, 54*(1), 1-10.

Sarhan, T., García-Lafuente, J., Vargas, M., Vargas, J. M., & Plaza, F. (2000). Upwelling mechanisms in the northwestern Alboran Sea. *Journal of Marine Systems, 23*(4), 317-331.

Sari, Y. D., Syaukat, K., Kusumastanto, T., & Hartoyo, S. (2018). Management of demersal fishery in the Arafura Sea: A bio-economic approach. *Jurnal Sosial Ekonomi Kelautan dan Perikanan, 13*(1), 43-57.

Schiller, A. (2011). Ocean circulation on the North Australian Shelf. *Continental Shelf Research, 31*(10), 1087-1095.

Sea-Bird Scientific. (2017). *Product manual SBE 19plus V2 SeaCAT profiler CTD.* Retrieved October 25, 2018, from https://www.seabird.com/asset-get.download.jsa?id=54627862329

Sprintall, J., & Liu, W. (2005). Ekman mass and heat transport. *Oceanography, 18*(4), 88-97.

Sproson, D., & Sahlée, E. (2014). Modelling the impact of Baltic Sea upwelling on the atmospheric boundary layer. *Tellus A: Dynamic Meteorology and Oceanography, 66*(1), 1-16.

Stewart, R. H. (2006). *Introduction to physical oceanography.* Texas, USA: Department of Oceanography, Texas A & M University.

Susanto, R. D., Gordon, A. L., & Zheng, Q. (2001). Upwelling along the coasts of Java and Sumatra and its relation to ENSO. *Geophysical Research Letters, 28*(8), 1599-1602.

Taufikurahman, Q., & Hidayat, R. (2017). Coastal upwelling in Southern Coast of Sumbawa Island, Indonesia. *IOP Conference Series: Earth and Environmental Science, 54*(1), 1-7.

Tomczak, M. (2014). *Lecture notes in oceanography.* California, USA: CreateSpace Independent Publishing Platform.

Tranchant, B., Reffray, G., Greiner, E., Nugroho, D., Koch-Larrouy, A., & Gaspar, P. (2015). Evaluation of an operational ocean model configuration at 1/12° spatial resolution for the Indonesian seas – Part 1: Ocean physics. *Geoscientific Model Development Discussions, 8*(8), 6611-6668.

Utama, F. G., Atmadipoera, A. S., Purba, M., Sudjono, E. H., & Zuraida, R. (2017). Analysis of upwelling event in Southern Makassar Strait. *IOP Conference Series: Earth and Environmental Science, 54*(1), 1-9.

Wattimena, M. C. (2020). *Structure and variability of the Indonesian throughflow in Halmahera Sea* (Doctorate Dissertation). IPB University, Indonesia.

Wilks, D. S. (2006). *Statistical methods in the atmospheric sciences* (2nd Ed.). New York, NY: Academic Press.

Worsfold, M., Good, S., Martin, M., McLaren, A., Robert-Jones, J., & Fiedler, E. (2020). *Global ocean OSTIA sea surface temperature reprocessing SST-GLO-SST-L4-REP-OBSERVATIONS-010-011.* Product user manual, Copernicus Marine Environment Monitoring Service. Retrieved June 20, 2020, from https://resources.marine.copernicus.eu/documents/PUM/CMEMS-SST-PUM-010-011.pdf

Wyrtki, K. (1961). *Physical Oceanography of the Southeast Asian Waters, Naga Report Volume 2.* San Diego, California: Scripps Institution of Oceanography, the University of California.